



## Competitive adsorption removal of indigo carmine and Congo red dyes from residual effluents by Zn<sub>2</sub>Al-LDH prepared by co-precipitation

Ali Bouteiba<sup>a,\*</sup>, Naceur Benhadria<sup>a</sup>, Abdelkader Elaziouti<sup>b</sup>, Karima Ezziane<sup>a</sup>,  
Nourredine Bettahar<sup>a</sup>

<sup>a</sup>Laboratoire de Chimie des Matériaux Inorganiques et Application-LCMIA, Université des Sciences et de la Technologie d'Oran (USTO M. B), B.P: 1505 El M'naouar, 31000 Oran, Algérie, Tel. +213 553168572; Fax: +213 45738927; emails: ali.bouteiba@usto.dz/ aliaiboutaiba@gmail.com (A. Bouteiba), naceur.benhadria@univ-usto.dz (N. Benhadria), ezziane.karima@univ-usto.dz (K. Ezziane), bettihar.nourredine@univ-usto.dz (N. Bettahar)

<sup>b</sup>Laboratoire des Sciences, Technologie et Génie des Procédés – LSTGP, Université des Sciences et de la Technologie d'Oran (USTO M. B), B.P: 1505 El M'naouar, 31000 Oran, Algérie, email: abdelkader.elaziouti@univ-usto.dz (A. Elaziouti)

Received 27 December 2019; Accepted 18 April 2020

### ABSTRACT

In this work, Zn<sub>2</sub>Al-LDH (layered double hydroxides) hydrotalcite was synthesized via co-precipitation method at pH = 9 and molar ratio Zn<sup>2+</sup>/Al<sup>3+</sup> of 2. The as-prepared LDH was characterized by X-ray diffraction, Fourier transform infrared, thermogravimetric analysis, N<sub>2</sub> adsorption-desorption isotherms, scanning electron microscopy, and pH (point of zero charge). The effective adsorption of Indigo carmine (IC) and Congo red (CR) from single and binary dye systems was assessed under various experimental keys parameters (adsorbent dosage, initial dye concentration, reaction time, pH solution, and temperature of the system). The First derivative spectrophotometric method was used to treat the adsorption data from the binary system. Results showed that the adsorption equilibrium of both dyes was reached within 60 min either in single or binary dye systems. The dynamical data of both dyes were well fitted with the pseudo-second-order kinetic model. All the explored temperatures showed that the adsorption process is endothermic and spontaneous. Besides, the equilibrium sorption data of dyes on both systems were well described with the modified Redlich-Peterson extended Freundlich and extended Sips. Zn<sub>2</sub>Al-LDH exhibited a greater affinity towards IC (162.87 mg/g) than that for the CR (25.11 mg/g) in a binary system. The adsorption mechanism was mainly monitored by electrostatic interactions between the positively charged LDH layer and negatively charged dyes molecules.

*Keywords:* Zn<sub>2</sub>Al-LDH; Dyes; Binary solution; Kinetics; Isotherms

### 1. Introduction

The water pollution from dyes industries is a major environmental problem. The presence of dyes even at low concentrations (less than 1 ppm) in the residual effluents may reduce the photosynthetic activity and increase toxicity. Moreover, these organic dyes are refractory, non-biodegradable, carcinogenic, and mutagenic, which create serious threats to human health as well as an

ecosystem [1]. Thus, the treatment and refinement of wastewaters via a judicious route are crucial. In the process of dye removal, various treatment methods such as chemical precipitation [2], membrane filtration [3], ion exchange [4], adsorption [5], photocatalysis, electrochemical degradation process [6], coagulation [7], and bio-removal technique have been developed [8]. Among these methods, adsorption is one of the best, efficient, low-cost, and green environmentally friendly route for this purpose. Due to its

\* Corresponding author.

structural characteristics and porous texture which give large surface area and great removal capacity for all kinds of pollutants, the commercial activated carbon is the most commonly used adsorbent for eliminating pollutions from water and air. However, the widespread use of activated carbon faces various challenges and limitations including a relatively high cost of production, and regeneration process difficulty [9]. To overcome these shortcomings, the need for more efficient and low-cost adsorbent via a judicious synthesis method is a subject of many kinds of research [10]. In this context, the layered double hydroxides (LDHs) also recognized as hydrotalcite-like materials have attracted much attention in recent years because of their robust structural properties, high surface area, non-toxicity, low cost, high thermal, and chemical stabilities [11]. The most striking aspect of these unique structures is their tendency to exchange the interlayer anions with different species that justify their potential applications in areas such as adsorption, pollution treatment, catalysis, photocatalysis, electronic, nanomedicine, agriculture, and drugs delivery.

These LDHs materials can be formulated as,  $[M_{1-x}^{2+} M_x^{3+}(\text{OH})_2]^{x+} (A^{n-})_{x/n} \cdot m\text{H}_2\text{O}$ , where  $M^{2+}$  is divalent ( $M^{2+} = \text{Mg}^{2+}, \text{Cu}^{2+}, \text{Zn}^{2+}$ , and so on) and  $M^{3+}$  is trivalent ( $M^{3+} = \text{Al}^{3+}, \text{Fe}^{3+}$ , and so on) metal cations,  $A^{n-}$  is inter-layer exchangeable anions such as  $\text{NO}_3^-$ ,  $\text{CO}_3^{2-}$ ,  $\text{Cl}^-$ , etc., and  $m$  is amount of water molecules [12]. The chemical composition of the LDHs can be tuned by changing the metal cations and the interlayer anions by commonly used synthetic methods like co-precipitation [13], urea hydrolysis, hydrothermal, and ion exchange [14].

In LDH systems, the  $M^{2+}/M^{3+}$  molar ratio value can be tuned in a relatively wide range without the main structural change. The upper limit of  $M^{2+}/M^{3+}$  value could be needed to prevent a collapse of the interlayer region due to a too long distance between these interlayer anions. In this case, the higher substitution of  $M^{2+}$  by  $M^{3+}$  within the brucite-like layer, greater the electrostatic attraction between the layers and the interlayer anions. This attraction causes the compression of the LDH structure. The lower limit of  $M^{2+}/M^{3+}$  value (if  $M^{2+}/M^{3+} \leq 2$ ) generally results in greater electrostatic repulsion of neighboring trivalent metal cations within the brucite-like layer and also the repulsion between the charge-balancing anions in the interlayer region [15]. To obtain pure phases of LDH and avoid the formation of single hydroxides, that is,  $\text{MII}(\text{OH})_2$  and  $\text{MIII}(\text{OH})_3$ , the  $M^{2+}/M^{3+}$  values must be constrained in a certain range from 2 to 4. In this range, the high performance of the LDH material can be achieved. LDHs such as  $\text{Zn}_2\text{Al}-\text{CO}_3$  LDH with  $\text{Zn}^{2+}/\text{Al}^{3+}$  molar ratio equal to 2 has been used in adsorption of acid and reactive dyes from wastewater [16] and to reduce metal toxicity such as As(III) and As(V) [17].

Many previous studies used a single dye aqueous solution for studying the efficiency of an adsorbent and did not consider the interaction that could exist in simulated multi-component adsorption systems. Therefore, a limited number of research papers have been reported about them. In the case of dyes, the study of the multicomponent dye adsorption systems is very important in terms of selectivity or affinity of each dye for a given adsorbent and competitively between dyes for the same surface adsorbent sites. Recently, some previous have been published for multicomponent dyes systems on different adsorbents

including the simultaneous removal of dyes from textile effluent using the nanocomposite material cobalt ferrite–alginate [18], surfactant modified nano- $\delta$ -alumina [19], competitive biosorption of dyes molecules onto inactive aerobic granules [20].

Therefore, based on the literature illustrations, our current study focuses on the elaboration of  $\text{Zn}_2\text{Al}-\text{CO}_3$  LDH material by the co-precipitation method at  $\text{pH} = 9$  and  $\text{Zn}^{2+}/\text{Al}^{3+}$  molar ratio of 2. The as-prepared LDH was characterized by various physicochemical techniques (X-ray diffraction (XRD), Fourier transform infrared (FT-IR), thermogravimetric analysis (TGA),  $\text{N}_2$  adsorption–desorption isotherms, scanning electron microscopy, and  $\text{pH}$  value at the point of zero charge ( $\text{pH}_{\text{pzc}}$ ).  $\text{Zn}_2\text{Al}$ -LDH was investigated as a potential material in the removal of two anionic dyes, Indigo carmine (IC) and Congo red (CR), as probe pollutants, in the single and binary adsorption systems from aqueous solution. Several experimental keys parameters such as reaction time, initial dye concentration, adsorbent dosage,  $\text{pH}$  solution, and temperature of the system were explored. Langmuir, Freundlich, Redlich–Peterson, Sips isotherms models, and their extended forms were applied to the experimental data. The experimental data were also analyzed by kinetic models (pseudo-first-order, pseudo-second-order, and intra-particle diffusion). The mechanism of the enhanced adsorption performances of  $\text{Zn}_2\text{Al}$ -LDH was elucidated in detail.

## 2. Experimental and method

### 2.1. $\text{Zn}_2\text{Al}$ -LDH synthesis

$\text{Zn}_2\text{Al}$ -LDH with molar ratio of 2 was prepared by the co-precipitation method at a fixed  $\text{pH} = 9$ . Experimentally, a mixed solution of  $\text{ZnCl}_2 \cdot 6\text{H}_2\text{O}$  (0.2 mol) and  $\text{AlCl}_3 \cdot 6\text{H}_2\text{O}$  (0.1 mol) in 100 mL of distilled water was prepared and was added dropwise under vigorous stirring to 100 mL solution of the salts (0.2 mol  $\text{Na}_2\text{CO}_3$  and 0.1 mol  $\text{NaOH}$ ). The  $\text{pH}$  solution of the co-precipitation process was maintained constant at  $\text{pH} = 9$  with the addition of  $\text{NaOH}$  solution. Afterward, the solution mixture was continuously stirred for 24 h at  $80^\circ\text{C}$  for maturation and then was centrifuged. This matured sol was washed with distilled water until obtaining a  $\text{Cl}^-$  free LDH ( $\text{AgNO}_3$  test) and dried for 24 h at  $65^\circ\text{C}$  to obtain the  $\text{Zn}_2\text{Al}-\text{CO}_3$  LDH and ground in an agate mortar [16].

### 2.2. Characterization methods $\text{Zn}_2\text{Al}$ -LDH

The TGA curve was recorded via a thermal analyzer (Inan apparatus) equipped with Mettler balances with a readability of  $\pm 0.1$  mg under nitrogen flow in the temperature range of  $25^\circ\text{C}$ – $1,000^\circ\text{C}$  and with a heating rate of  $10^\circ\text{C}/\text{min}$ . XRD analysis was done by Bruker D8 advance diffractometer (Germany) with  $\text{CuK}$  radiation ( $\lambda = 0.15406$  nm) over a  $2\theta$  range of  $7^\circ$ – $70^\circ$ . FT-IR spectra were carried out by using a Tensor 27 spectrometer (Bruker Optik GmbH, Germany) in the wavenumber range of  $400$ – $4,000$   $\text{cm}^{-1}$ . Brunauer–Emmett–Teller (BET) specific surface area, pore volume, and average pore diameter of the LDH sample were determined by  $\text{N}_2$  adsorption–desorption ( $77$  K)

method (Micromeritics Tristar 3000, Germany) after degassing the sample in a vacuum under nitrogen flow at 150°C. The morphology and structure properties were investigated with Quinta 250 SEM at 20–12.5 keV. The so-called pH drift method was used to determine the  $\text{pH}_{\text{pzc}}$  of LDH. In a typical assay, 25 mg of LDH was mixed with 25 mL of NaCl (0.1 M) at room temperature and then was adjusted to successive initial pH values between 2 and 12 with the addition of HCl and NaOH. Afterward, the resulting suspensions were stirred for 24 h at room temperature and the final pHs were measured. The pH value at the point of zero charges was determined by plotting the difference between final and initial pH ( $\Delta\text{pH}$ ) vs. the initial pH [21].

### 2.3. Adsorption procedure

The adsorption experiments for the single-component solution was conducted by using 0.04 g of the  $\text{Zn}_2\text{Al}$ -LDH added to a series of 250 mL Erlenmeyer flasks filled with 20 mL of 100 mg/L IC or CR solution at 25°C. The effects of pH solution (2–12), adsorbent dosages (0.01–0.1 g), the temperature of the system (298–328 K) and initial dye concentrations (100–800 mg/L) for IC and (50–500 mg/L) for CR solutions on LDH adsorption capacity were studied.

For binary systems, the same procedure in the above single system was used. Except for the initial dye concentration ratio of 100:100 mg/L for each dye in the mixture was used. To investigate the influence of dye concentration on the removal efficiency of IC in the presence of CR dye, a varying concentration of IC range 100–800 mg/L was mixed with a fixed concentration of CR 20, 50, 80, and 100 mg/L, and a varying concentration of CR range 50–500 mg/L was mixed with a fixed concentration of IC 20, 50, 80, and 100 mg/L.

The effects of adsorption parameters in single and binary systems were examined at 25°C, and the amount of dye adsorbed and dye removal percentage was determined as follows [22]:

$$Q_{ei} = \frac{(C_0 - C_e)}{m} \times V \quad (1)$$

$$R\% = \frac{(C_0 - C_e)}{C_0} \times 100 \quad (2)$$

where  $Q_{ei}$  is the amount of dye adsorbed per unit weight of adsorbent (mg/g);  $C_0$  and  $C_e$  are the initial and equilibrium dye concentrations (mg/L), respectively;  $V$  is the dye volume used in adsorption process (L);  $m$  is the mass of  $\text{Zn}_2\text{Al}$ -LDH (g), and  $R$  is the dye removal percentage (%).

To determine the best fitting kinetic model, we use the chi-square parameter ( $\chi^2$ ):

$$\chi^2 = \sum_{i=1}^N \frac{(Q_{e \text{ exp}} - Q_{e \text{ cal}})^2}{Q_{e \text{ cal}}} \quad (3)$$

where  $Q_{e \text{ exp}}$  is the equilibrium adsorption capacity from the experiment (mg/g);  $Q_{e \text{ cal}}$  is the equilibrium capacity calculated according to the model (mg/g).

The solution samples were taken at regular time intervals during the adsorption process. The residual dye concentrations were determined by Shimadzu UV/vis-1700 spectrophotometer (Japan).

To investigate the dye removal efficiency in multi-component adsorption systems, the dye solutions in the concentration range of 4–12 mg/L of each dye were prepared and analyzed with the UV-visible spectrophotometer to get a zero-order absorption spectrum (Fig. 1a). Fig. 1a shows the difference in the absorption spectrum of IC and CR dyes in their pure and binary solutions. The maximum absorbencies of IC and CR dyes in their pure solutions were obtained at 610 and 500 nm, respectively. However, the direct measurement of IC and CR dye in binary solutions would be inaccurate because of the overlapping spectra. To resolve this problem, the derivative spectrophotometric method was adopted for binary solutions. Fig. 1b shows the first-order derivative absorption spectra against wavelength ( $\lambda$ ) of IC and CR in a single and binary mixture.

Therefore, in the presence of both dyes, the absorbance of each dye can be determined at a specific wavelength, where the absorbance of the other dye is zero; and thus the absorbance of CR dye can be localized at 480 nm, while for IC dye it can be determined at 630 nm and then the concentration of each dye was calculated from the calibration curves obtained at similar concentrations (Fig. 2).

### 2.4. Single and multicomponent adsorption equilibrium isotherms

The adsorption segment was focused by using four normal isotherms to correlate the adsorption results of the explored dyes onto our LDHs, explicitly the Freundlich, Langmuir, Redlich–Peterson, and Sips isotherms which are formed as follows.

#### 2.4.1. Langmuir isotherm

$$Q_{ei} = \frac{Q_{\text{max}i} K_{Li} C_e}{1 + K_{Li} C_e} \quad (4)$$

where  $Q_{ei}$  is the equilibrium adsorption capacity for component  $i$  (mg/g),  $C_e$  is the equilibrium concentration (mg/L),  $Q_{\text{max}i}$  and  $K_{Li}$  are the maximum adsorption capacity for component  $i$  (mg/g), and Langmuir constant for component  $i$  (L/mg), respectively [23].

The Langmuir isotherm model can be applied to multi-component systems to get different forms such as non-modified Langmuir multicomponent isotherm (NLMI), modified Langmuir multicomponent isotherm (MLMI) with an interaction factor  $\eta_i$ , and extended Langmuir multicomponent isotherm (ELMI).

#### 2.4.2. Non-modified Langmuir multicomponent isotherm

$$Q_{ei} = \frac{Q_{\text{max}i} K_{Li} C_{ei}}{1 + \sum_{i=1}^N K_{Li} C_{ei}} \quad (5)$$

where  $Q_{\text{max}i}$  and  $K_{Li}$  are the maximum adsorption capacity for component  $i$  (mg/g) and Langmuir constant for component

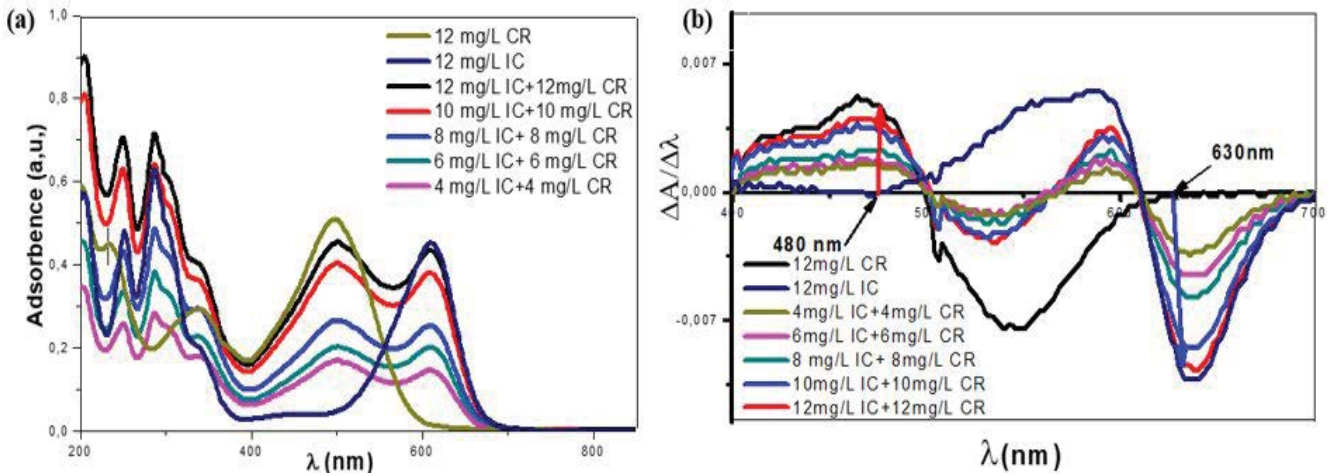


Fig. 1. (a) Zero-order adsorption spectra of dyes in single and binary solutions. (b) First-order derivative spectra of dyes in the range of 4–12 mg/L of CR and IC concentrations in binary systems.

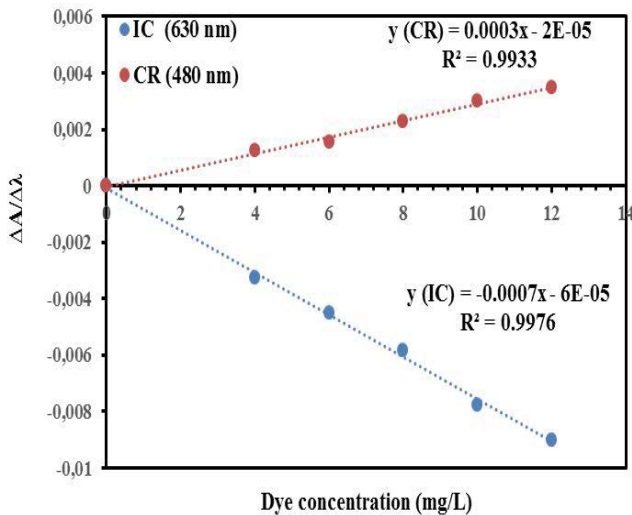


Fig. 2. Calibration curve of first-order derivative spectra for binary system.

(L/mg), respectively, calculated from the experimental data of individual Langmuir isotherms, and  $N$  is the total number of components in the solution [24].

Modified Langmuir multicomponent isotherm (MLMI) with an interaction factor  $\eta_i$ :

$$Q_{ei} = \frac{Q_{\text{Emax}i} K_{\text{EL}i} (C_{ei} / \eta_i)}{1 + \sum_{i=1}^N K_{\text{EL}i} (C_{ei} / \eta_i)} \quad (6)$$

where  $\eta_i$  is the interaction factor for dye  $i$  [24].

#### 2.4.3. Extended Langmuir multicomponent isotherm

$$Q_{ei} = \frac{Q_{\text{Emax}i} K_{\text{EL}i} C_{ei}}{1 + \sum_{i=1}^N K_{\text{EL}i} C_{ei}} \quad (7)$$

For a solution containing two components, the adsorption capacity  $Q_{e(\text{IC})}$ ,  $Q_{e(\text{CR})}$  can be calculated using the following equations.

$$Q_{e(\text{IC})} = \frac{Q_{\text{Emax}(\text{IC})} K_{\text{EL}(\text{IC})} C_{e(\text{IC})}}{1 + K_{\text{EL}(\text{IC})} C_{e(\text{IC})} + K_{\text{EL}(\text{CR})} C_{e(\text{CR})}} \quad (8)$$

$$Q_{e(\text{CR})} = \frac{Q_{\text{Emax}(\text{CR})} K_{\text{EL}(\text{CR})} C_{e(\text{CR})}}{1 + K_{\text{EL}(\text{CR})} C_{e(\text{CR})} + K_{\text{EL}(\text{IC})} C_{e(\text{IC})}} \quad (9)$$

where  $Q_{e\text{max}i}$  and  $K_{\text{EL}i}$  are the extended maximum adsorption capacity for component  $i$  (mg/g) and extended Langmuir constant for component  $i$  (L/mg), respectively [24].

#### 2.4.4. Freundlich isotherm

$$Q_{ei} = K_{fi} C_{ei}^{1/n_{fi}} \quad (10)$$

where  $K_{fi}$  is the Freundlich isotherm constant for dye  $i$  (mg/g)  $(\text{L/mg})^{1/n_{fi}}$  and  $n_{fi}$  is the Freundlich isotherm constant for dye  $i$ .

The extended Freundlich isotherm model for the multicomponent system (EFIM) can be represented as [24]:

$$Q_{e(\text{IC})} = \frac{K_{f(\text{IC})} C_{e(\text{IC})}^{1/n_{f(\text{IC})} + X_{(\text{IC})}}}{C_{e(\text{IC})}^{X_{(\text{IC})}} + Y_{(\text{IC})} C_{e(\text{CR})}^{2/(n_{f(\text{IC})})}} \quad (11)$$

$$Q_{e(\text{CR})} = \frac{K_{f(\text{CR})} C_{e(\text{CR})}^{1/n_{f(\text{CR})} + X_{(\text{CR})}}}{C_{e(\text{CR})}^{X_{(\text{CR})}} + Y_{(\text{CR})} C_{e(\text{IC})}^{2/(n_{f(\text{CR})})}} \quad (12)$$

The values of Extended Freundlich constants for both dyes:  $X_{(\text{IC})}$ ,  $Y_{(\text{IC})}$ ,  $Z_{(\text{IC})}$ ,  $X_{(\text{CR})}$ ,  $Y_{(\text{CR})}$ ,  $Z_{(\text{CR})}$  are obtained from the experimental data of the multicomponent system.

#### 2.4.5. Redlich–Peterson isotherm

Redlich–Peterson isotherm is derived by combining both the Langmuir and Freundlich isotherm models and the model equation is developed by taking all the model constants [25]. The equation can be given as:

$$Q_{ei} = \frac{a_i C_{ei}}{1 + b_i C_{ei}^{\beta_i}} \quad (13)$$

where  $\beta_i$  is the Redlich–Peterson isotherm constant for dye ( $0 < \beta \leq 1$ ),  $a_i$  is the Redlich–Peterson isotherm constant for dye (L/g) and  $b_i$  is the Redlich–Peterson isotherm constant for dye (L/mg) $^{\beta}$ .

The Redlich–Peterson model can be applied to multi-component systems to get different forms such as competitive non-modified (NRPMI) and modified Redlich–Peterson multicomponent isotherm (MRPMI) with an interaction factor  $\eta_i$  [25].

The non-modified competitive Redlich–Peterson isotherm is expressed as:

$$Q_{ei} = \frac{a_i C_{ei}}{1 + \sum_{i=1}^N b_i C_{ei}^{\beta_i}} \quad (14)$$

The modified Redlich–Peterson multicomponent isotherm (MRPMI) with an interaction factor  $\eta_i$  is expressed as:

$$Q_{ei} = \frac{a_i (C_{ei} / \eta_i)}{1 + \sum_{i=1}^N b_i (C_{ei} / \eta_i)^{\beta_i}} \quad (15)$$

where  $a_i$ ,  $b_i$ , and  $\beta_i$  are the model constants which are obtained from the experimental data of individual Redlich–Peterson isotherms.

#### 2.4.6. Sips isotherm

The Sips model is another empirical model for representing equilibrium adsorption data. It is a combination of the Langmuir and Freundlich isotherm type models. The Sips model takes the following form for single solute equilibrium data [26]:

$$Q_{ei} = \frac{Q_{\max i} (k_{\text{sps}} C_{ei})^{\text{ms}}}{1 + (k_{\text{sps}} C_{ei})^{\text{ms}}} \quad (16)$$

where  $K_{\text{sip}}$  is the Sips constant related to the energy of adsorption (L/mg) and ms is the parameter characterizing the heterogeneity of the adsorption system.

For multi-component adsorption systems, the Sips multicomponent adsorption isotherm model can be written as [26]:

$$Q_{ei} = \frac{Q_{\max i} (k_{\text{sps}} C_{ei})^{\text{ms}}}{1 + \sum_{i=1}^N (k_{\text{sps}} C_{ei})^{\text{ms}}} \quad (17)$$

### 3. Results and discussion

#### 3.1. Characterization of Zn<sub>2</sub>Al-LDH

The XRD patterns of as-synthesized Zn<sub>2</sub>Al-LDH are depicted in Fig. 3a. All the diffraction peaks can be indexed as (0 0 3), (0 0 6), (1 0 1), (0 1 5), (0 1 8), (1 1 0), and (1 1 3) basal reflections of planes of a hexagonal lattice with 3R rhombohedral symmetry (JCPDS card No. 38–0486), usually applied for the description of the LDH structure. The basal spacing of 7.57 Å for Zn<sub>2</sub>Al-LDH corresponding to the prominent reflection (0 0 3), indicates the basal reflection of an interlayer anion species in LDH material. The first peak of the doublet at  $2\theta = 60^\circ$  is due to the crystallography orientation from the (110) planes, and its spacing corresponds to the lattice parameter “a,” which coincides with the closest M–M distance in the brucite-like layers. The average crystallite size and specific surface area for Zn<sub>2</sub>Al-LDH were found to be 25.68 nm and 185.495 m<sup>2</sup>/g, respectively. The unit cell parameters “a” and “c” can be calculated from the positions of these reflections: “a” = 2d<sub>110</sub> and “c” = 3d<sub>003</sub>. The obtained parameters are presented in Table 1. These lattice parameters agree well with those reported for hydrotalcite-like compounds [27].

Fig. 3b displays the infrared spectra of the sample before adsorption between 4,000 and 400 cm<sup>-1</sup>. It resembles that of other hydrotalcite-like phases with CO<sub>3</sub><sup>2-</sup> as the counter anions. The broadband observed at 3,441 cm<sup>-1</sup> is attributed to the interlayer water molecules. The weak band at 1,620 cm<sup>-1</sup> is due to the bending vibration (deformation mode of H–O–H ( $\delta$  H–O–H)) of interlayer water molecules in LDH. The strong band at 1,359 cm<sup>-1</sup> is due to the mode  $\nu_3$  of the interlayer carbonate species as reported in the literature, the bands in the range of 500–750 cm<sup>-1</sup> are related to Zn–O, Al–O, and metal-oxygen–metal vibrational modes in brucite-type layer [28].

TGA analyses were applied to determine the thermal stability of the prepared sample. As shown in Fig. 3c, three distinct weight losses were observed, namely 20% in the range of 50°C–250°C, 7% from 250°C to 650°C and 2% from 650°C to 1,000°C. These weight losses were attributed to the loss of physically adsorbed and interlayer water. The second weight loss was due to the first step of dihydroxylation and the removal of carbonates ions from the interlayer. In the third weight loss, the hydrotalcite undergoes carbonation and dihydroxylation reactions and produce metal oxides. The total weight losses of the sample in the temperature range up to 700°C are approximately 29%.

The SEM images of this compound are shown in Fig. 4. As can be seen from Figs. 4a–c the particles of Zn<sub>2</sub>Al-LDH are precipitated as small, pseudo-spherical aggregates of platelets, the diameters of the particles vary from 200 to 220 nm.

The porosity properties and specific surface area of the Zn<sub>2</sub>Al-LDH were assessed through the N<sub>2</sub> sorption measurements at 77 K. Obviously, the N<sub>2</sub> adsorption–desorption isotherms for LDH were categorized as type IV (Fig. S1a) with a typical H3 type hysteresis loop reflecting that the mesoporous structure is formed due to the irregular agglomeration of the plate-like samples according to the IUPAC classification [29]. Moreover, near a relative pressure of 1, no plateau was observed, indicating the coexistence of macropores. The pore size distribution calculated by using

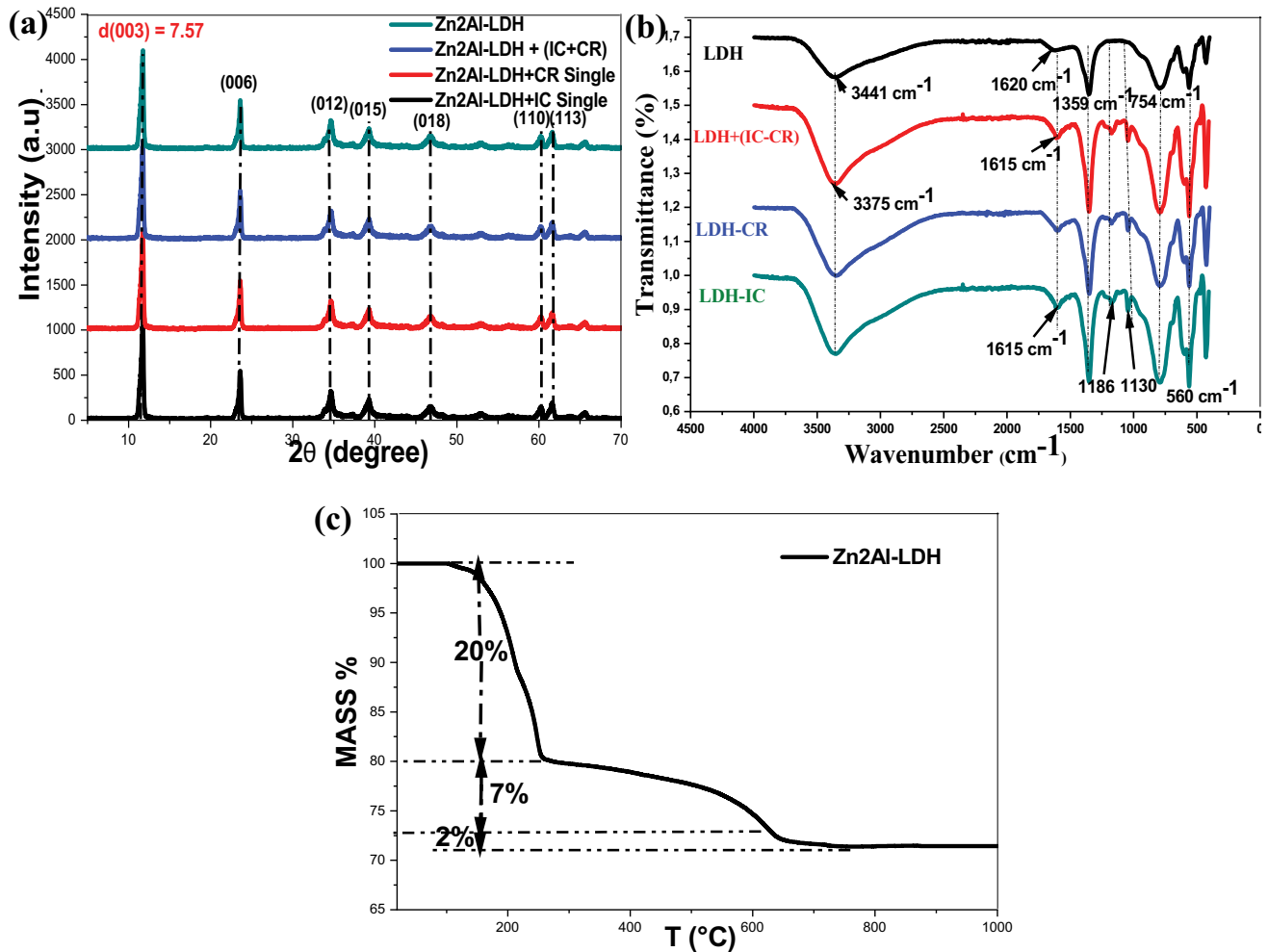


Fig. 3. (a) XRD patterns, (b) FTIR spectra of the  $Zn_2Al-LDH$  material before and after adsorption of IC and CR in single and binary systems, and (c) thermogravimetric analysis.

Table 1  
Unit cell parameters and interlamellar distance of  $Zn_2Al-LDH$

Sample	$Zn_2Al-LDH$
$a$ (Å)	3.08
$c$ (Å)	22.71
Interlamellar distance (Å)	7.57

the Barrett–Joyner–Halenda (BJH) model with the adsorption branch, as displayed in Fig. S1b, shows that the average pore diameter of LDH is within the range of 3.79–5.68 nm. Owing to these features, the synthesized LDH materials are highly suitable to be used as adsorbents for anionic dye. The BET surface area, average pore volume, and average pore diameter of the adsorbents are summarized in Table 2.

### 3.2. Effect of adsorbent dosage

The effect of adsorbent dosage on the adsorption efficiency of  $Zn_2Al-LDH$  was investigated and the

corresponding curves are presented in Fig. S2. The removal efficiency of IC and CR dyes in single and binary systems increased with increasing  $Zn_2Al-LDH$  dosage up to 0.04 g. This is due to the increase in adsorbent surface area and availability of more adsorption surface sites stemming from the increased dose. Besides, a decrease in dyes removal in the binary system, which might be ascribed to the interference and competitive effects of the specific sites on the adsorbent surface [16]. However, at higher adsorbent doses, beyond 0.04 g, no significant changes in removal efficiency were observed. Therefore 0.04 g was chosen as the optimum adsorbent dose for further study.

### 3.3. Effect of pH solution

The pH of the solution is one of the most important parameters that control the efficiency of the sorption process. The effect of the initial pH on the adsorption of CR and IC in single and binary solution is shown in Fig. S3. It is noted that the total dye removal was maximum and almost constant in the range at pH 2–9 in single and binary solutions. Conversely, increasing the pH value beyond 10,

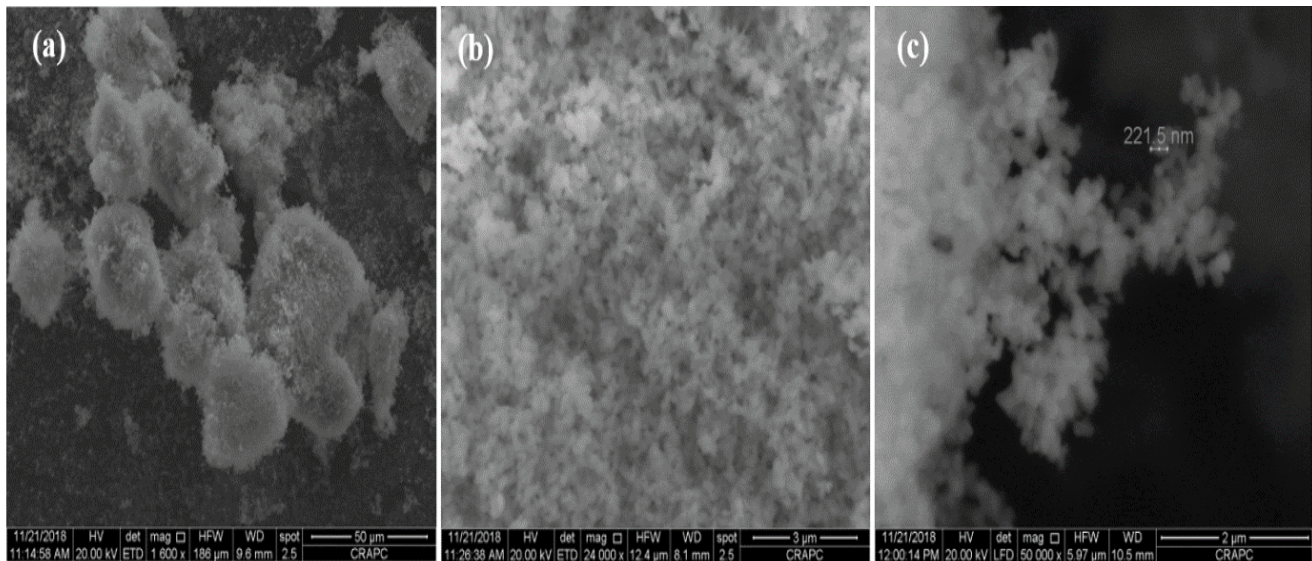


Fig. 4. SEM images of  $Zn_2Al$ -LDH material.

Table 2  
Physical characteristics of  $Zn_2Al$ -LDH

Adsorbent	$Zn_2Al$ -LDH
Specific surface area (m <sup>2</sup> /g)	185.495
Average pore volume (cm <sup>3</sup> /g)	0.294
Average pore diameter (nm)	56.80
Crystallite size (nm)*	25.68

\*Calculated from XRD

a dramatic decline in dye removal was observable. These results can be explained in terms of surface charge properties of the  $Zn_2Al$ -LDH material. Fig. S4 displays the distribution curve of the point charge zero ( $pH_{pzc}$ ) for  $Zn_2Al$ -LDH with the measured value of 10. At  $pH > 10$  the surface of the material is negatively charged, favoring the adsorption of cationic molecules. While at  $pH < 10$ , the surface acquires a positive charge, preferring the adsorption of anionic molecules [21,30]. Indeed, at pH values in the range of 2–9 ( $pH < pH_{pzc} = 10$ ), strong adsorption of CR and IC on the LDH is evident, due to the electrostatic attraction of the positive charge of LDH and the negative charge of the dyes molecules, resulting in greatest adsorption efficiency. However, the removal efficiency is scarcely reduced at highly alkaline pH ( $pH \geq pH_{pzc} = 10$ ), primarily ascribed to the electrostatic repulsion between analogously charged species. On the base of the above results,  $pH = 7$  was selected as optimum for all further studies.

### 3.4. Competitive adsorption

#### 3.4.1. Effect of initial dye concentration

In the application of adsorption for purification of wastewater, the solution will normally be a mixture of many compounds rather than a single one. The interactions of these compounds may mutually enhance or mutually

inhibit adsorption capacity. As can be seen in Fig. 5, the capacity of  $Zn_2Al$ -LDH for adsorbing IC is higher than that of CR. For example, the amount of IC and CR adsorbed on LDH was 184 and 145 mg/g, respectively, when the concentration of the dye at equilibrium was 132 mg/L. Thus, the  $Zn_2Al$ -LDH adsorption capacity toward IC was 1.26 times greater than that towards CR.

#### 3.4.2. Effect of contact time and initial dye concentration

An increase in initial dye concentration decreases the dye adsorption capacity from single to a binary system, as recorded in Table 3. The adsorbed capacity of dyes on  $Zn_2Al$ -LDH in single solution increased from 19.9 to 49 mg/g for IC and from 16.1 to 46.8 mg/g for CR within 60 min of contact time. The maximum adsorption capacity of IC and CR on LDH in a single solution was 49 and 46.8 mg/g, respectively. However, the adsorption capacity of each dye in the binary system was decreased to 44.7 and 35.9 mg/g in the presence of 50 and 100 mg/L of CR, respectively. A similar trend was also observed in the case of mixture solutions for the removal of CR in the presence of IC. The adsorbed quantity of CR on LDH was reduced from 46.8 to 39 mg/g as the initial concentration of IC was increased up to 50 mg/L and almost reached 27.75 mg/g in the occurrence of 100 mg/L of IC. So, the presence of the other dye develops competitive adsorption for unoccupied sites on the surface. The adsorption rate of IC and CR on LDH at different dye concentrations in single and binary systems was examined at various contact times in the range of 0–60 min. Results indicate that the uptake of IC and CR was rapid at the initial 10 min of contact time and then continued to increase until reaching equilibrium after 55–60 min. Zolgharnein et al. [31] showed that only 200 min is sufficient to reach equilibrium during the competitive adsorption of IC in binary dyes system on CTAB-modified  $TiO_2$  nanoparticles. The initial dye concentration had no pronounced effect on the equilibrium time.

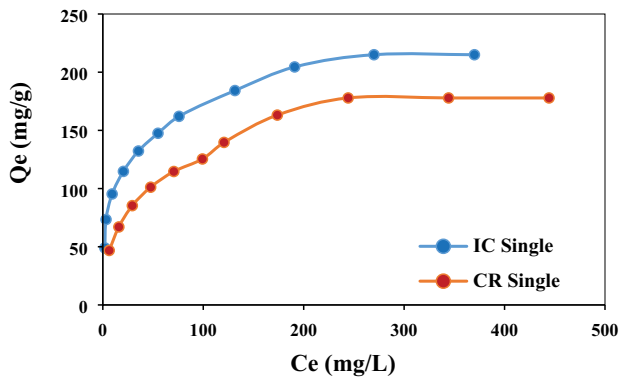


Fig. 5. Adsorption isotherms for IC and CR in single solution system.

3.4.3. Relative adsorption and selectivity

Relative adsorption was calculated using the following equation [20]:

$$Ar = \frac{[Q_t]_B}{[Q_t]_S} \tag{18}$$

where  $[Q_t]_B$  (mg/g) and  $[Q_t]_S$  (mg/g) are the adsorption capacities of each dye in the binary and single systems at time  $t$ , respectively.

The selectivity of the IC against CR in the binary system was evaluated as follows:

$$S = \frac{(Ar)_{IC}}{(Ar)_{CR}} \tag{19}$$

where  $(Ar)_{IC}$  and  $(Ar)_{CR}$  are the relative adsorptions of IC and CR, respectively.

The variation of relative adsorption of IC and CR and the adsorption selectivity in dyes mixture as a function of time is shown in Fig. 6. The results indicate a gradual increase in the relative adsorption of CR molecules. This means that the dynamic uptake process of CR is significantly influenced by the presence of IC dye. The selectivity values of adsorption decreased and approached a constant value of 1. This can be attributed to the higher affinity of  $Zn_2Al$ -LDH

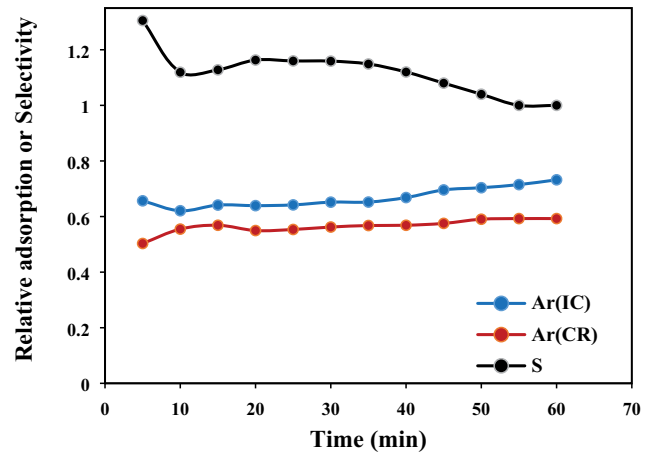


Fig. 6. Relative adsorption and adsorption selectivity for dyes in binary system.

to IC molecules in the binary system. When the adsorption approaches the equilibrium, the adsorption selectivity will be the same for IC and CR, the adsorption results suggest that the presence of IC has a significant influence on CR adsorption capacity, while IC adsorption including capacity and kinetics is affected by the presence of CR.

3.4.4. Adsorption kinetics models in single and binary dyes systems

In this present study, three kinetic models are used to define the adsorption mechanism onto the  $Zn_2Al$ -LDH surface. These models include the pseudo-first-order, pseudo-second-order, and intra-particle diffusion.

3.4.4.1. Pseudo-first order model

The experimental kinetic data are investigated by the pseudo-first-order model according to Lagergren's equation [16]:

$$\ln(Q_e - Q_{et}) = \ln(Q_e) - k_1 t \tag{20}$$

where  $k_1$  is the rate constant (1/min) and  $Q_t$  is adsorption capacity at time  $t$  (mg/g). Hence, the values of  $k_1$  and  $Q_e$  are

Table 3  
Kinetic parameters for the adsorption of IC and CR on LDH in single and binary systems

Dye	Experimental	Pseudo-first-order model				Pseudo-second-order model				
	$Q_{e,exp}$ (mg/g)	$Q_{e,cal}$ (mg/g)	$k_1$ (1/min)	$R^2$	$\chi^2$	$Q_{e,cal}$ (mg/g)	$k_2 \times 10^{-5}$ (g/mg/min)	$h$ (mg/g/min)	$R^2$	$\chi^2$
IC Single <sup>a</sup>	49	25.28	0.0639	0.96	22.3	52.63	2.903	222.701	0.99	0.25
IC Binary <sup>b</sup>	44.7	26.92	0.0772	0.89	11.8	48.31	5.5	299.433	0.99	0.26
IC Binary <sup>c</sup>	35.9	17.77	0.057	0.94	18.5	39.37	12.8	308.449	0.99	0.31
CR Single <sup>a</sup>	46.8	44.54	0.1045	0.91	0.12	50.5	3.897	253.495	0.99	0.27
CR Binary <sup>b</sup>	39.0	25.51	0.0544	0.93	7.15	42.74	7.1	236.924	0.99	0.32
CR Binary <sup>c</sup>	27.8	24.32	0.0532	0.94	0.48	30.49	25.1	216.699	0.99	0.25

<sup>a</sup>(100 mg/L), <sup>b</sup>(100:50 mg/L), and <sup>c</sup>(100:100 mg/L).

deduced from the slope ( $k_1$ ) and the intercept ( $\ln(Q_e)$ ) of the linear plots of  $\ln(Q_e - Q_t)$  vs.  $t$  for the adsorption of IC and CR on  $\text{Zn}_2\text{Al-LDH}$  at various dye concentration ratios studied.

#### 3.4.4.2. Pseudo-second-order model

The kinetic data were further analyzed using the pseudo-second-order model, as follows [32]:

$$\frac{t}{Q_{et}} = \frac{1}{K_2 Q_e^2} + \frac{1}{Q_e} t \quad (21)$$

where  $k_2$  is the rate constant ( $\text{g/mg/min}$ ) model. Thus, the plot of  $t/Q_{et}$  versus  $t$ , at all the dye concentration ratios studied, give straight line whose slope and intercept are equal to  $1/Q_e$  and  $1/Q_e^2 K_2$ , respectively.

The initial sorption rate  $h$  ( $\text{mg g}^{-1} \text{min}^{-1}$ ) was calculated when  $t$  approximates to zero, as follows:

$$h = K_2 Q_e^2 \quad (22)$$

Then Eq. (22) becomes:

$$\frac{t}{Q_{et}} = \frac{1}{h} + \frac{1}{Q_e} t \quad (23)$$

Kinetic parameters of the pseudo-first-order and pseudo-second-order models jointly with the correlation coefficients

( $R^2$ ) and chi-square parameter ( $\chi^2$ ) for the adsorption of IC and CR on  $\text{Zn}_2\text{Al-LDH}$  adsorbent at all the dye concentration studied, are presented in Table 3.

#### 3.4.4.3. Intra-particle diffusion study

The adsorption process is also described by the intra-particle diffusion model suggested by Weber and Morris [33] in the following expression:

$$Q_{et} = K_d t^{1/2} + C \quad (24)$$

where  $Q_t$  is the amount of solute on the surface of the adsorbent at time  $t$  ( $\text{mg/g}$ ),  $K_d$  is the intra-particle rate constant ( $\text{mg/g min}^{1/2}$ ),  $t$  is the time ( $\text{min}$ ), and  $C$  ( $\text{mg/g}$ ) is a constant that gives an idea about the thickness of the boundary layer. The values of  $K_d$  and  $C$  for different dye concentrations are calculated from the linear plot of  $Q_{et}$  vs.  $t^{1/2}$  (Figs. 7a and b).

On the base of the kinetic modeling, as presented in Tables 3 and 4, the experimental data fit better with the pseudo-second-order model with high correlation coefficients ( $R^2 > 0.99$ ) of both dyes. Moreover, the chi-square parameter values  $\chi^2$  are smaller than 1.89%. The calculated  $Q_e$  values are almost closer to the experimental data, indicating that the adsorption process is controlled by a chemical adsorption process. Besides, from the initial sorption rate  $h$ ,  $\text{Zn}_2\text{Al-LDH}$  adsorbs IC faster than CR in both single and

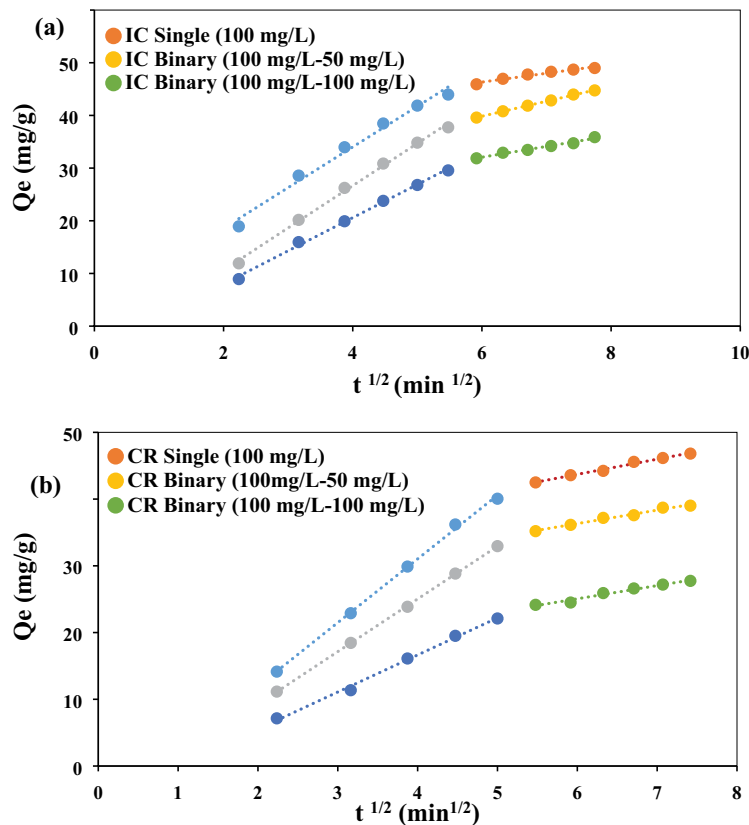


Fig. 7. Intra-particle diffusion model for (a) IC and (b) CR adsorption in single and binary systems.

Table 4  
Kinetic parameters for intra-particle diffusion of IC and CR on LDH in single and binary systems

Dye	Intra-particle diffusion model		
	$K_{id}$ (mg/g/min <sup>0.5</sup> )	C (mg/g)	$R^2$
IC Single <sup>a</sup>	1.669	36.319	0.965
IC Binary <sup>b</sup>	2.842	22.795	0.999
IC Binary <sup>c</sup>	2.045	19.785	0.984
CR Single <sup>a</sup>	2.268	30.101	0.99
CR Binary <sup>b</sup>	2.015	24.239	0.985
CR Binary <sup>c</sup>	1.975	13.211	0.976

<sup>a</sup>(100 mg/L), <sup>b</sup>(100:50 mg/L), and <sup>c</sup>(100:100 mg/L).

binary systems. This highlight can be explained in terms of the molecule size of the explored dyes. Indeed, the IC molecule is smaller size as compared to that of CR.

On the other hand, the pseudo-first-order model ( $0.96 > R^2 > 0.89$ ) is not a suitable model for describing the adsorption kinetics for all dye concentration ratios. The calculated and experimental values  $Q_e$  diverged significantly.

As can be seen from Figs. 7a and b the adsorption of both dyes onto LDH in the single and binary solution can be well fitted by the intra-particle diffusion model ( $R^2 > 0.997$ ). The plots consisted of two linear sections indicating that two steps contribute to the adsorption process. Step “one” is the diffusion through the solution to the external surface of the adsorbent or the boundary layer diffusion of solute molecules, while step “two” corresponds to the ongoing adsorption stage, where intra-particle diffusion is the rate-limiting step. The first portions of straight lines do not pass through the origin, indicating that intra-particle diffusion is not the only limiting step, and other steps also influence the rate of mass transfer [34].

As shown in Table 4, the value of the C parameter decreased in the presence of both dyes as a function of dye concentration, while the intra-particle diffusion rate constant increased. Similar results were reported by Sun et al. [35]. This suggests that high initial concentration provides an important driving force to overcome all mass transfer resistances of dye between the aqueous and solid phases [36]. In particular, at this level of dyes concentration, there has been a competition for these adsorption sites on the surface.

### 3.4.5. Effect of temperature

The effect of temperature (in the range 298–328 K) on the adsorption of both dyes on Zn<sub>2</sub>Al-LDH in single and binary solutions is investigated at various initial dye concentration ratios IC: CR of 100:0, 0:100, and 100:100 (mg/L:mg/L). The removal efficiency for both dyes increases with increasing temperature from 298 to 328 K, suggesting that the adsorption process is endothermic. The thermodynamic parameters were determined by the following equations [16].

$$k = \frac{Q_{ei}}{C_{ei}} \quad (25)$$

$$\Delta G^\circ = \Delta H^\circ - T\Delta S^\circ \quad (26)$$

$$\ln K = \left( -\frac{\Delta H^\circ R}{T} \right) - \left( \frac{\Delta S^\circ}{R} \right) \quad (27)$$

where K is the equilibrium constant,  $\Delta G^\circ$  is the variation in the Gibbs free energy (kJ/mol),  $\Delta H^\circ$  is the thermal energy of the reaction (kJ/mol),  $\Delta S^\circ$  is the variation in the randomized energy (J/mol K), T is the absolute temperature (K), and R is the universal gas constant (8.314 J/mol K). By plotting  $\ln K$  vs.  $1/T$ , the values of  $\Delta H^\circ$  and  $\Delta S^\circ$  are determined from the slope ( $-\Delta H^\circ R$ ) and intercept ( $\Delta S^\circ R$ ). The thermodynamic parameters ( $\Delta H^\circ$ ,  $\Delta S^\circ$ , and  $\Delta G^\circ$ ) obtained at all the temperatures studied for the adsorption of both dyes on Zn<sub>2</sub>Al-LDH in single and binary solutions at optimum initial dye concentration are listed in Table 5. The positive values of  $\Delta H^\circ$  for both dyes mean that the adsorption process is endothermic and physical. The positive values of  $\Delta S^\circ$  indicate an increase in the randomness at the solid/liquid interface. The negative values of  $\Delta G^\circ$  reveal that IC and CR adsorption process on Zn<sub>2</sub>Al-LDH is feasible and spontaneous [37].

### 3.4.6. Adsorption isotherms in single and binary component systems

The Langmuir, Freundlich, Redlich–Peterson, and Sips isotherms were fitted to the experimental adsorption equilibrium data for a single dye on Zn<sub>2</sub>Al-LDH. The experimental equilibrium adsorption data were obtained by varying

Table 5  
Thermodynamic parameters for adsorption of IC and CR on LDH in single and binary systems

	$\Delta G^\circ$ (KJ/mol)					
	$\Delta H^\circ$ (KJ/mol)	$\Delta S^\circ$ (KJ/mol K)	T (K)			
			298	308	318	328
IC Single <sup>a</sup>	1.698	0.42	-123.462	-127.662	-131.862	-136.062
IC Binary <sup>b</sup>	0.14	0.034	-9.99	-10.332	-10.672	-11.012
CR Single <sup>a</sup>	0.633	0.163	-47.941	-49.571	-51.201	-52.831
CR Binary <sup>b</sup>	0.178	0.016	-4.59	-4.75	-4.91	-5.07

<sup>a</sup>(100 mg/L), <sup>b</sup>(100:100 mg/L)

the concentrations of IC or CR with a fixed dosage of LDH. The adsorption parameters for each dye in the single solution obtained from the fitting of different isotherm models with the experimental data are listed in Table 6 along with the correlation coefficient values ( $R^2$ ), the sum of squares due to the errors (SSE), and root means square errors (RMSE), as shown in Fig. 8.

One can see those regression coefficients obtained from the Freundlich, Redlich–Peterson, and Sips isotherms are similar and higher than those of the Langmuir isotherm for LDH, which suggests the heterogeneous adsorption of IC and CR on LDH. The maximum adsorption of IC and CR are 207.96 and 193.5 mg/g, respectively, based on the Langmuir isotherm.

For the binary solution, the fitted parameter values are listed in Table 7 and the model curves are plotted in Figs. 9 and 10. The multicomponent adsorption equilibrium data were interpreted with the three multicomponent adsorption models based on the Langmuir isotherm. The values of the  $R^2$  and SSE shown in Table 7 indicated that the NLMI, the MLMI, and ELMI cannot fit the experimental data since the squares due to the errors SSE are very high for both dyes (80 for IC and 98 for CR) and the obtained correlation coefficients ( $R^2$ ) are less than 0.875. The non-modified (NRPMI) and MRPMI were well fitted to the experimental adsorption equilibrium data, but the SSE of the NRPMI was lower than that of the MRPMI model, as displayed in Table 7.

For example, the MRPMI presented an SSE of 5.65 for the IC–CR system, whereas the SSE of NRPMI was 3.85. This result was attributed to the fact that the NRPMI comprised six parameters from the single component Redlich–Peterson isotherms; meanwhile, the MRPMI included the same parameters from the single component Redlich–Peterson isotherms and two interaction factors related to the multicomponent interactions. In other words, the MRPMI better fitted the data because the multicomponent interactions were

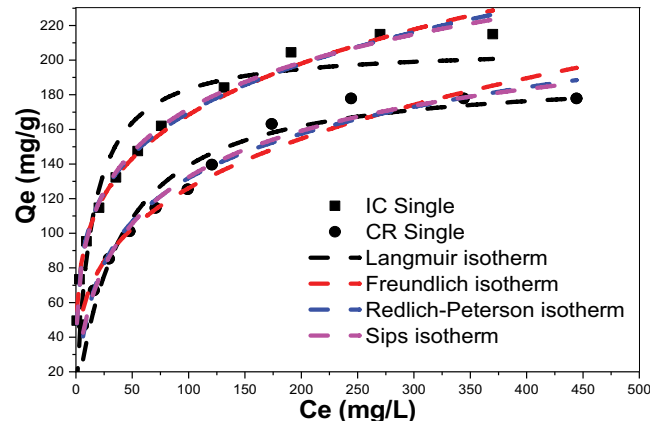


Fig. 8. Isotherm plots of the adsorption of IC and CR on  $Zn_2Al$ -LDH in single system with different models.

Table 6

Parameter values of the Langmuir, Freundlich, Redlich–Peterson, and sips isotherms for non-linear for the single dye adsorption

Isotherm model	Number of parameters	Parameter values	
		IC	CR
Langmuir	2	$Q_{max} = 207.958$ (mg/g) $K_L = 0.074$ (L/mg) $R^2 = 0.939$ RMSE = 7.263 SSE = 25.85	$Q_{max} = 193.5$ (mg/g) $K_L = 0.026$ (L/mg) $R^2 = 0.976$ RMSE = 2.586 SSE = 5.348
Freundlich	2	$K_f = 57.326$ (mg/g) (L/mg) <sup>1/n</sup> $n_f = 4.273$ $R^2 = 0.994$ RMSE = 2.851 SSE = 2.225	$K_f = 32.511$ (mg/g) (L/mg) <sup>1/n</sup> $n_f = 3.398$ $R^2 = 0.979$ RMSE = 2.37 SSE = 2.839
Redlich–Peterson	3	$a = 62.674$ (L/g) $b = 0.84$ (L/mg) <sup>β</sup> $β = 0.817$ $R^2 = 0.995$ RMSE = 2.268 SSE = 2.226	$a = 11.54$ (L/g) $b = 0.45$ (L/mg) <sup>β</sup> $β = 0.794$ $R^2 = 0.988$ RMSE = 2.368 SSE = 3.348
Sips	3	$Q_{max} = 484.499$ (mg/g) $K_{sip} = 0.002$ (L/mg) $ms = 0.338$ $R^2 = 0.989$ RMSE = 2.845 SSE = 3.345	$Q_{max} = 208.468$ (mg/g) $K_{sip} = 0.02$ (L/mg) $ms = 0.922$ $R^2 = 0.986$ RMSE = 2.475 SSE = 3.215

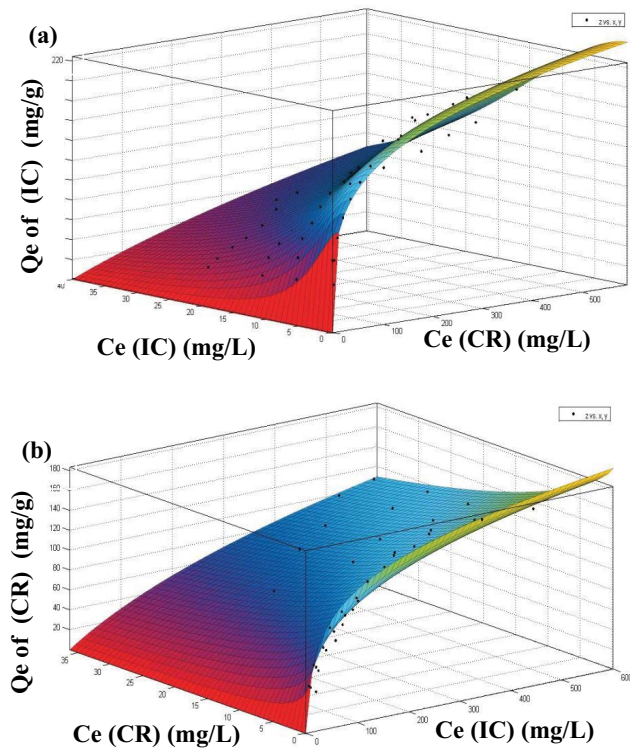


Fig. 9. Binary adsorption isotherms (a) of IC with CR and (b) of CR with IC on LDH. The surfaces are predicted with the MRPMI model.

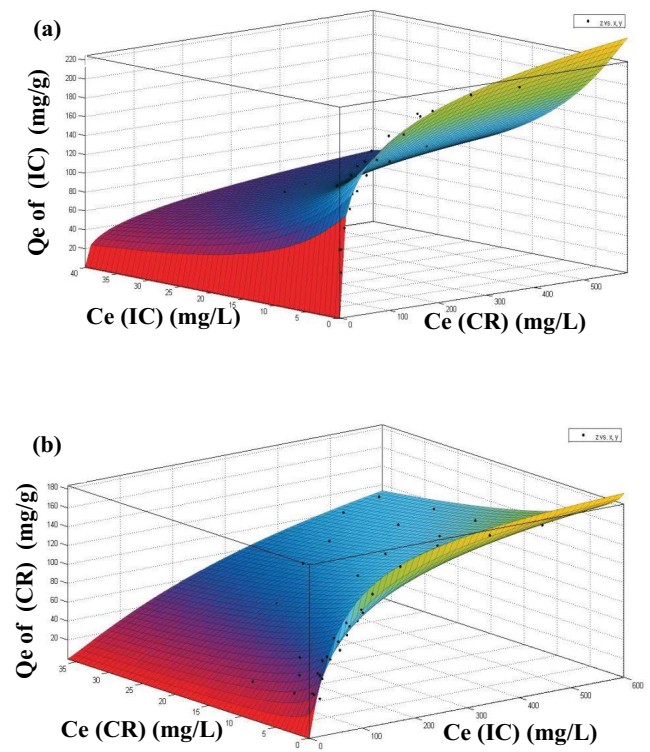


Fig. 10. Binary adsorption isotherms (a) of IC with CR and (b) of CR with IC on LDH. The surfaces are predicted with the Sips model.

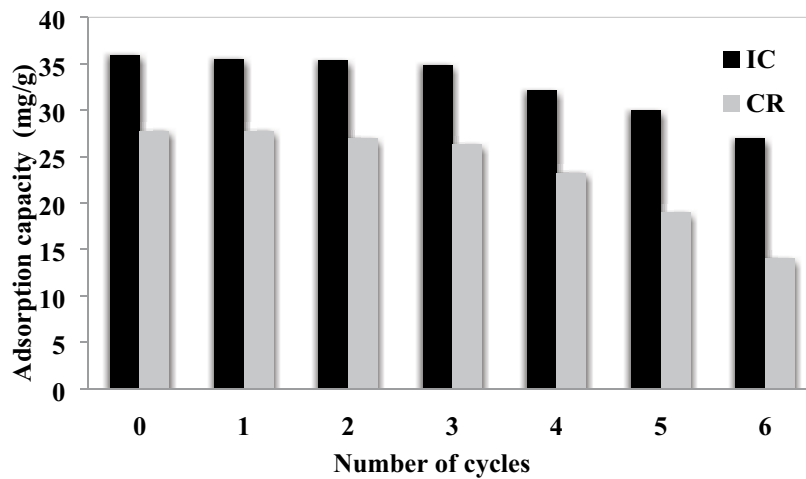


Fig. 11. Adsorption capacity of dye mixture in Zn<sub>2</sub>Al-LDH according to the number of the cycle of washing/adsorption.

incorporated into this model. This is why the MRPMI model was chosen over the NRPMI model. The obtained results for the CR–IC system were the same. The interpretation of the multicomponent experimental data was also performed with the extended Freundlich multi-component isotherm (EFMI) and extended Sips. Both isotherm models used single component isotherm parameters and various interaction competition factors. For the IC–CR system, the SSE and  $R^2$  of EFMI were, respectively, 1.26 and 0.998, whereas that of

extended Sips was 2.16 and 0.988. For the CR–IC system, the SSE and  $R^2$  of EFMI were 3.22 and 0.989, respectively. Whereas that of extended Sips was 2.92 and 0.988.

The adsorption capacity of various adsorbents recently reported in the literature are compared with the present study and their predicted values of  $Q_{max}$  are displayed in Table 8. It can be seen that Zn<sub>2</sub>Al-LDH exhibited a high adsorption capacity toward IC dye in both single and binary systems. Meanwhile, for CR dye, the results showed an

Table 7  
Parameter values of the Langmuir, Freundlich, Redlich–Peterson, and Sips isotherms for the binary dye adsorption

Isotherm model	Single isotherm parameters	Interaction factors	Parameter values	
			IC	CR
(NLMI)	4	0	$R^2 = 0.873$ RMSE = 10.6 SSE = 80.07	$R^2 = 0.683$ RMSE = 14.31 SSE = 98
(ELMI)	0	3	$Q_{\text{max}} = 187.62$ (mg/g) $K_{\text{EL(IC)}} = 0.095$ $K_{\text{EL(CR)}} = 1.07$ $R^2 = 0.875$ RMSE = 12.75 SSE = 75.87	$Q_{\text{max}} = 25.11$ (mg/g) $K_{\text{EL(CR)}} = 0.51$ $K_{\text{EL(IC)}} = 0.18$ $R^2 = 0.85$ RMSE = 5.26 SSE = 70.7
(MLMI) with an interaction factor $\eta_i$	4	2	$\eta_{\text{(IC)}} = 0.962$ $\eta_{\text{(CR)}} = 0.029$ $R^2 = 0.88$ RMSE = 9.96 SSE = 71.93	$\eta_{\text{(CR)}} = 1.08$ $\eta_{\text{(IC)}} = 0.19$ $R^2 = 0.85$ RMSE = 3.68 SSE = 71.31
(EFMI)	4	3	$X_{\text{(IC)}} = 0.503$ $Y_{\text{(IC)}} = 0.225$ $Z_{\text{(IC)}} = 1.464$ $R^2 = 0.997$ RMSE = 2.211 SSE = 1.26	$X_{\text{(CR)}} = 0.988$ $Y_{\text{(CR)}} = 1.633$ $Z_{\text{(CR)}} = 0.903$ $R^2 = 0.989$ RMSE = 2.43 SSE = 3.22
(NRPMI)	6	0	$R^2 = 0.948$ RMSE = 2.263 SSE = 3.85	$R^2 = 0.95$ RMSE = 3.211 SSE = 2.3
(MRPM) with an interaction factor $\eta_i$	6	2	$\eta_{\text{(IC)}} = 1.218$ $\eta_{\text{(RC)}} = 0.329$ $R^2 = 0.986$ RMSE = 2.261 SSE = 5.65	$\eta_{\text{(CR)}} = 1.03$ $\eta_{\text{(IC)}} = 3.41$ $R^2 = 0.987$ RMSE = 3.171 SSE = 3.742
Extended Sips	6	0	$R^2 = 0.988$ RMSE = 2.36 SSE = 2.16	$R^2 = 0.988$ RMSE = 2.49 SSE = 2.92

interesting adsorption capacity in comparison with that of the Bentonite and Mg–Fe–CO<sub>3</sub> LDH. On the other hand, the adsorption capacities of Go–NiFe LDH, hierarchical porous Ni/Co-layered double hydroxide (NiCo-LDH) hollow dodecahedra, and the hierarchical NH<sub>4</sub>Al(OH)<sub>2</sub>CO<sub>3</sub>Ni(OH)<sub>2</sub> microfibers toward CR single solution system are very higher than the Zn<sub>2</sub>Al-LDH.

### 3.5. Adsorption mechanism

To study the adsorption mechanism, the structure of Zn<sub>2</sub>Al-LDH after adsorption experiments was further characterized by XRD and FT-IR techniques. As we can see from Fig. 3a, the interlayer distance  $d_{003}$  was not modified as a consequence of the adsorption of the dyes ( $\approx 7.57$  Å), therefore the dyes were not effectively intercalated in the interlayer. This finding can be explained by the presence of carbonate anions in the interlayer space. Indeed, in our

case, the exceptionally high affinity of LDH toward carbonate anions makes the ion-exchange mechanism of other anions very difficult and in some cases, only physisorption involving weak forces can take place. This result was expected for carbonate-intercalated LDH, as reported by other studies [38]. Besides, the FT-IR bands analysis, shown in Fig. 3b, revealed the presence of several new bands at 1,130; 1,186; and 1,615 cm<sup>-1</sup>, attributing to the vibration of C–N, symmetric stretching vibrations of the sulfonic acid group (–SO<sub>3</sub><sup>-</sup>) and the vibration of –N=N–, respectively. This highlight can be related to the electrostatic interaction between anionic functional groups of the dyes and the positively charged surface of Zn<sub>2</sub>Al-LDH adsorbent [39].

### 3.6. Desorption and regeneration

It is very important to study the stability and the performance of the obtained adsorbents in several cycles. Fig. 12

Table 8  
Comparison between adsorption capacities of IC and CR for different adsorbents

Adsorbent	Dye	$Q_{\max}$ (mg/g)	Reference
CTAB-modified $\text{TiO}_2$	IC	106.24	[31]
Mg/Fe LDH	IC	55.5	[40]
Cobalt hydroxide nanoparticles	IC	163	[41]
$\text{Zn}_2\text{Al-LDH}$	IC binary	162.87	In this study
$\text{Zn}_2\text{Al-LDH}$	IC single	207.96	In this study
Mg-Fe- $\text{CO}_3$ LDH	CR	104.6	[42]
GO-NiFe LDH	CR	489	[43]
Hierarchical $\text{NH}_4\text{Al}(\text{OH})_2\text{CO}_3@ \text{Ni}(\text{OH})_2$ microfibers	CR	426	[44]
Bentonite	CR	13.16	[45]
$\text{Zn}_2\text{Al-LDH}$	CR Single	74.78	In this study
$\text{Zn}_2\text{Al-LDH}$	CR Binary	25.11	In this study
NiCo-LDH	CR	909.2	[46]
Natural clay	CR	61.12	[47]

shows the evaluation of the adsorptive capacity of dye using  $\text{Zn}_2\text{Al-LDH}$  in six successive adsorption cycles. To extract the dye molecules from the adsorbent surface, three solvents (methanol, water, and 50% methanol + 50% water) were used. The methanol solvent presented the highest desorption capacity since 95% of IC and 90% of CR were desorbed at room temperature within 2 h, indicating that both dyes molecules had greater affinity to methanol.

The regenerated  $\text{Zn}_2\text{Al-LDH}$  particles from the methanol solvent were shaken in water to remove the remained traces of methanol, separated by centrifugation, and then dried at 65°C overnight. The obtained  $\text{Zn}_2\text{Al-LDH}$  sample was reused for six adsorption–desorption cycles by using methanol as eluent, during the sixth cycles, the amount adsorbed by washed  $\text{Zn}_2\text{Al-LDH}$  of dyes mixture with ratio 100/100 mg/L decreased from  $\approx 35.87$  to 27 mg/g for IC and from 27.75 to 14 mg/g for CR. During the first three cycles, it is indicated that the  $\text{Zn}_2\text{Al-LDH}$  does not lose its activity toward both dyes, while a slight reduction of its performance was observed during the three remaining cycles.

#### 4. Conclusion

In summary, the co-precipitation method was used to prepare  $\text{Zn}_2\text{Al-LDH}$  at the  $\text{Zn}^{2+}/\text{Al}^{3+}$  molar ratio of 2 for effective adsorption of IC and CR from single and binary dyes solutions. Results showed that  $\text{Zn}_2\text{Al-LDH}$  is a hexagonal lattice with 3R rhombohedral symmetry and basal spacing of 7.57 Å. The average crystallite size and specific surface area were found to be 25.68 nm and 185.495  $\text{m}^2/\text{g}$ , respectively.  $\text{Zn}_2\text{Al-LDH}$  exhibited substantial adsorption efficiency of IC and CR from single and binary systems within 60 min. The experimental data are well described by the pseudo-second-order model with high correlation coefficients ( $R^2 > 0.99$ ). Based on the thermodynamical results, the adsorption is endothermic, feasible, and spontaneous. Furthermore, the experimental results in single systems are well fitted with the non-linear isotherms Freundlich, Redlich–Peterson, and Sips while the extended models: EFML, MRPMI, and Sips in mixture solutions.

The adsorption affinity of IC on  $\text{Zn}_2\text{Al-LDH}$  in a single system was privileged than that of CR while it decreased in the binary system.  $\text{Zn}_2\text{Al-LDH}$  demonstrated great stability after three regeneration cycles. The removal performances of the  $\text{Zn}_2\text{Al-LDH}$  for both dyes were progressively reduced during the sixth adsorption–desorption cycles. The enhanced adsorption capacity of the  $\text{Zn}_2\text{Al-LDH}$  was primarily ascribed to the electrostatic attraction of the positive charge of LDH and the negative charge of the dyes molecules, in single and binary systems.

#### Acknowledgments

We would like to especially thank the laboratory members (Laboratoire de chimie des matériaux inorganique et applications (LCMIA), Faculté de Chimie, Université des Sciences et de la Technologie d'Oran Mohamed Boudiaf (USTO-MB)) who contributed to this work.

#### References

- [1] A.R. Bagheri, M. Ghaedi, S. Hajati, A.M. Ghaedi, A. Goudarzi, A. Asfaram, Random forest model for the ultrasonic-assisted removal of chrysoidine G by copper sulfide nanoparticles loaded on activated carbon; response surface methodology approach, *RSC Adv.*, 5 (2015) 59335–59343.
- [2] C.R. Li, Z.Y. Zhuang, F. Huang, Z.C. Wu, Y.P. Hong, Z. Lin, Recycling rare earth elements from industrial wastewater with flowerlike nano- $\text{Mg}(\text{OH})_2$ , *ACS Appl. Mater. Interfaces*, 5, (2013) 9719–9725.
- [3] W. Liu, Z.L. Wu, Y.J. Wang, Y.L. Zhao, W.C. Liu, Y. Yu, Recovery of is flavones from the soy whey wastewater using two-stage batch foam fractionation, *Ind. Eng. Chem. Res.*, 52 (2013) 13761–13767.
- [4] L. Fu, C. Shuang, F. Liu, A. Li, Y. Li, Y. Zhou, H. Song, Rapid removal of copper with magnetic poly-acrylic weak acid resin: quantitative role of bead radius on ion exchange, *J. Hazard. Mater.*, 272 (2014) 102–111.
- [5] S. Zhao, D. Chen, F. Wei, N. Chen, Z. Liang, Y. Luo, Removal of Congo red dye from aqueous solution with nickel-based metalorganic framework/graphene oxide composites prepared by ultrasonic wave-assisted ball milling, *Ultrason. Sonochem.*, 39 (2017) 845–852.

- [6] A.M.S. Solano, S. Garcia-Segura, C.A. Martinez-Hustle, E. Brillas, Degradation of acidic aqueous solutions of the diazo dye Congo red by photo-assisted electrochemical processes based on Fenton's reaction chemistry, *Appl. Catal., B*, 169 (2015) 559–571.
- [7] X. Huang, X. Bo, Y. Zhao, B. Gao, Y. Wang, S. Sun, Q. Yue, Q. Li, Effects of compound biofloculant on coagulation performance and floc properties for dye removal, *Bioresour. Technol.*, 165 (2014) 116–121.
- [8] B.E. Taştan, S.E. Karatay, G. Dönmez, Bioremoval of textile dyes with different chemical structures by *Aspergillus versicolor* in molasses medium, *Water Sci. Technol.*, 66 (2012) 2177–2184.
- [9] C.M. Zhang, W. Song, G.H. Sun, L.J. Xie, L. Wan, J.L. Wang, K.X. Li, Synthesis, characterization, and evaluation of activated carbon spheres for dibenzothiophene from model diesel fuel, *Ind. Eng. Chem. Res.*, 53 (2014) 4271–4276.
- [10] S. Nayab, A. Farrukh, Z. Oluz, E. Tuncel, S.R. Tariq, H.U. Rahman, K. Kirchoff, H. Duran, B. Yameen, Design and fabrication of branched polyamine functionalized mesoporous silica: an efficient absorbent for water remediation, *ACS Appl. Mater. Interfaces*, 6 (2014) 4408–4417.
- [11] N. Benselka-Hadj Abdelkader, A. Bentouamib, Z. Derriche, N. Bettahar, L.C. de Menorval, Synthesis and characterization of Mg-Fe layer double hydroxides and its application on adsorption of Orange G from aqueous solution, *Chem. Eng. J.*, 169 (2011) 231–238.
- [12] P.S. Ghosal, A.K. Gupta, Enhanced efficiency of ANN using nonlinear regression for modeling adsorptive removal of fluoride by calcined Ca–Al–(NO<sub>3</sub>)–LDH, *J. Mol. Liq.*, 222 (2016) 564–570.
- [13] X. He, X. Qiu, C. Hu, Y. Liu, Treatment of heavy metal ions in wastewater using layered double hydroxides: a review, *J. Dispersion Sci. Technol.*, 39 (2018) 792–801.
- [14] L. Frederick, A.T. Godwin, L.A. Ray, Frost, Synthesis of layered double hydroxides containing Mg<sup>2+</sup>, Zn<sup>2+</sup>, Ca<sup>2+</sup> and Al<sup>3+</sup> layer cations by co-precipitation methods—a review, *Appl. Surf. Sci.*, 383 (2016) 200–213.
- [15] B. Balcomb, M. Singh, S. Singh, Synthesis and characterization of layered double hydroxides and their potential as nonviral gene delivery vehicles, *ChemistryOpen*, 4 (2015) 137–145.
- [16] I. Clark, J. Smith, R.L. Gomes, E. Lester, Continuous synthesis of Zn<sub>2</sub>Al–CO<sub>3</sub> layered double hydroxides for the adsorption of reactive dyes from water, *J. Environ. Chem. Eng.*, 7 (2019) 103175.
- [17] L. Shen, X. Jiang, Z. Chen, D. Fu, Q. Li, T. Ouyang, Y. Wang, Chemical reactive features of novel amino acids intercalated layered double hydroxides in As(III) and As(V) adsorption, *Chemosphere*, 176 (2017) 57–66.
- [18] R. Jayalakshmi, J. Jeyanthi, Simultaneous removal of binary dye from textile effluent using cobalt ferrite-alginate nanocomposite: performance, and mechanism, *Microchem. J.*, 145 (2019) 791–800.
- [19] J. Zolgharnein, M. Bagtash, T. Shariatmanesh, Simultaneous removal of a binary mixture of Brilliant Green and Crystal Violet using derivative spectrophotometric determination, multivariate optimization and adsorption characterization of dyes on surfactant modified nano- $\delta$ -alumina, *Spectrochim. Acta, Part A*, 137 (2015) 1016–1028.
- [20] J.F. Gao, Q. Zhang, K. Su, J.H. Wang, Competitive biosorption of Yellow 2G and Reactive Brilliant Red K-2G onto inactive aerobic granules: simultaneous determination of two dyes by first-order derivative spectrophotometry and isotherm studies, *Bioresour. Technol.*, 101 (2010) 5793–5801.
- [21] D. Chebli, A. Bouguettoucha, A. Reffas, C. Tiar, M. Boutahala, H. Gulyas, A. Amrane, Removal of the anionic dye Biebrich scarlet from water by adsorption to calcined and non-calcined Mg–Al layered double hydroxides, *Desal. Water Treat.*, 57 (2016) 22061–22073.
- [22] S. Ziane, F. Bessaha, K. Marouf-Khelifa, A. Khelifa, Single and binary adsorption of reactive black 5 and Congo red on modified dolomite: performance and mechanism, *J. Mol. Liq.*, 249 (2018) 1245–1253.
- [23] I. Langmuir, The adsorption of gases on plane surfaces of glass, mica and platinum, *J. Am. Chem. Soc.*, 40 (1918) 1361–1403.
- [24] M. Ghaedi, S. Hajjati, Z. Mahmudi, I. Tyagi, S. Agarwal, A. Maity, V.K. Gupta, Modeling of competitive ultrasonic-assisted removal of the dyes - methylene blue and safranin-O using Fe<sub>3</sub>O<sub>4</sub> nanoparticles, *Chem. Eng. J.*, 268 (2015) 28–37.
- [25] V.C. Srivastava, I.D. Mall, I.M. Mishra, Modelling individual and competitive adsorption of cadmium(II) and zinc(II) metal ions from aqueous solution onto bagasse fly ash, *Sep. Sci. Technol.*, 41 (2006) 2685–2710.
- [26] S. Nethaji, A. Sivasamy, B. Mandal, Adsorption isotherms, kinetics and mechanism for the adsorption of cationic and anionic dyes onto carbonaceous particles prepared from *Juglans regia* shell biomass, *Int. J. Environ. Sci. Technol.*, 10 (2013) 231–242.
- [27] F. Kefif, K. Ezziane, A. Bahmani, N. Bettahar, S. Mayouf, Evans Blue dye removal from contaminated water on calcined and uncalcined Cu–Al–CO<sub>3</sub> layered double hydroxide materials prepared by coprecipitation, *Bull. Mater. Sci.*, 42 (2019) 1–11.
- [28] C. Lei, M. Pi, P. Kuang, Y. Guo, F. Zhang, Organic dye removal from aqueous solutions by hierarchical calcined Ni–Fe layered double hydroxide: isotherm, kinetic and mechanism studies, *J. Colloid Interface Sci.*, 496 (2017) 158–166.
- [29] R.A.W. Sing, K.S.W. Everet, D.H. Haul, Provisional international union of pure and applied chemistry commission on colloid and surface chemistry subcommittee on reporting gas adsorption data \* reporting physisorption data for gas/solid systems with special reference to the determination of S, *Pure Appl. Chem.*, 57 (1985) 603–619.
- [30] Y. Al-Degs, M.A.M. Khraisheh, S.J. Allen, M.N. Ahmad, G.M. Walker, Competitive adsorption of reactive dyes from solution: equilibrium isotherm studies in single and multi-solute systems, *Chem. Eng. J.*, 128 (2007) 163–167.
- [31] J. Zolgharnein, M. Bagtash, N. Asanjarani, Hybrid central composite design approach for simultaneous optimization of removal of alizarin red S and indigo carmine dyes using cetyltrimethylammonium bromide-modified TiO<sub>2</sub> nanoparticles, *J. Environ. Chem. Eng.*, 2 (2014) 988–1000.
- [32] Y.S. Ho, G. McKay, Pseudo-second order model for sorption processes, *Process Biochem.*, 34 (1999) 451–465.
- [33] J. Fu, Z. Chen, M. Wang, S. Liu, J. Zhang, J. Zhang, R. Han, Q. Xu, Adsorption of methylene blue by a high-efficiency adsorbent (polydopamine microspheres): kinetics, isotherm, thermodynamics and mechanism analysis, *Chem. Eng. J.*, 259 (2015) 53–61.
- [34] I.A.W. Tan, B.H. Hameed, Adsorption isotherms, kinetics, thermodynamics and desorption studies of basic dye on activated carbon derived from oil palm empty fruit bunch, *J. Appl. Sci.*, 10 (2010) 2565–2571.
- [35] D. Sun, X. Zhang, Y. Wu, T. Liu, Kinetic mechanism of competitive adsorption of disperse dye and anionic dye on fly ash, *Int. J. Environ. Sci. Technol.*, 10 (2013) 799–808.
- [36] F. Banat, S. Al-Asheh, L. Al-Makhadmeh, Evaluation of the use of raw and activated date pits as potential adsorbents for dye containing waters, *Process Biochem.*, 39 (2003) 193–202.
- [37] S. Khamparia, D. Jaspal, Study of decolorization of binary dye mixture by response surface methodology, *J. Environ. Manage.*, 201 (2017) 316–326.
- [38] A. Guzmán-Vargas, E. Lima, G.A. Uriostegui-Ortega, M.A. Oliver-Tolentino, E.E. Rodríguez, Adsorption and subsequent partial photodegradation of methyl violet 2B on Cu/Al layered double hydroxides, *Appl. Surf. Sci.*, 363 (2016) 372–380.
- [39] S. Yang, L. Wang, X. Zhang, W. Yang, G. Song, Enhanced adsorption of Congo red dye by functionalized carbon nanotube/mixed metal oxides nanocomposites derived from layered double hydroxide precursor, *Chem. Eng. J.*, 275 (2015) 315–321.
- [40] M.A. Ahmed, A.A. brick, A.A.A. Mohamed, An efficient adsorption of indigo carmine dye from aqueous solution on mesoporous Mg/Fe layered double hydroxide nanoparticles prepared by controlled sol-gel route, *Chemosphere*, 174 (2017) 280–288.

- [41] J. Zolgharnein, M. Rastgordani, Optimization of simultaneous removal of binary mixture of indigo carmine and methyl orange dyes by cobalt hydroxide nano-particles through Taguchi method, *J. Mol. Liq.*, 262 (2018) 405–414.
- [42] I.M. Ahmed, M.S. Gasser, Adsorption study of anionic reactive dye from aqueous solution to Mg-Fe-CO<sub>3</sub> layered double hydroxide (LDH), *Appl. Surf. Sci.*, 259 (2012) 650–656.
- [43] Y. Zheng, B. Cheng, W. You, J. Yu, W. Ho, 3D hierarchical graphene oxide-Ni-Fe LDH composite with enhanced adsorption affinity to Congo red, methyl orange and Cr(VI) ions, *J. Hazard. Mater.*, 369 (2019) 214–225.
- [44] Y. Zheng, H. Wang, B. Cheng, W. You, J. Yu, Fabrication of hierarchical bristle-grass-like NH<sub>4</sub>-Al(OH)<sub>2</sub>CO<sub>3</sub>@Ni (OH)<sub>2</sub> core-shell structure and its enhanced Congo red adsorption performance, *J. Alloys Compd.*, 750 (2018) 644–654.
- [45] R. Pleșa Chicinaș, H. Bedelea, R. Stefan, A. Măicăneanu, Ability of a montmorillonite clay to interact with cationic and anionic dyes in aqueous solutions, *J. Mol. Struct.*, 1154, (2018) 187–195.
- [46] H. Hu, J. Liu, Z. Xu, L. Zhang, B. Cheng, W. Ho, Hierarchical porous Ni/Co-LDH hollow dodecahedron with excellent adsorption property for Congo red and Cr(VI) ions, *Appl. Surf. Sci.*, 478 (2019) 981–990.
- [47] S. Bentahar, A. Dbik, M. El Khomri, N. El Messaoudi, A. Lacherai, Adsorption of methylene blue, crystal violet and Congo red from binary and ternary systems with natural clay: kinetic, isotherm, and thermodynamic, *J. Environ. Chem. Eng.*, 5 (2017) 5921–5932.

Supplementary information

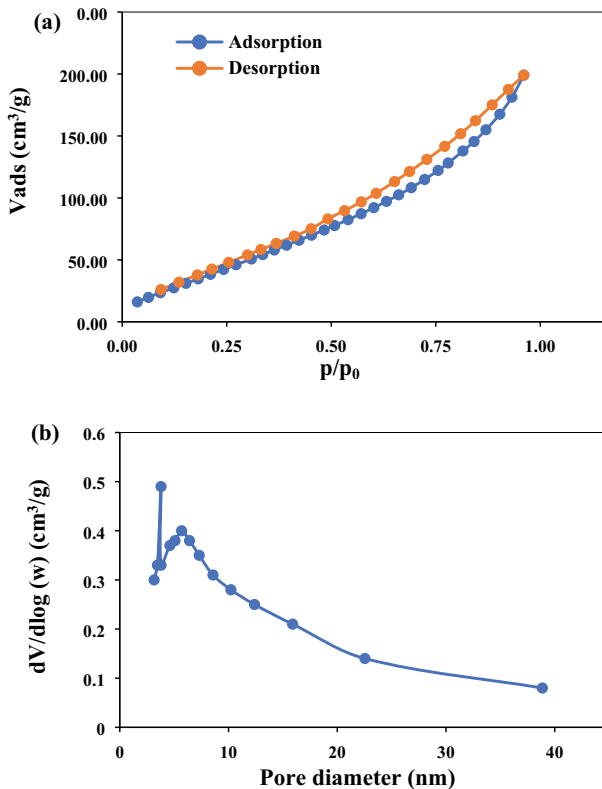


Fig. S1. (a) N<sub>2</sub> adsorption–desorption isotherms and (b) pore size distribution curves.

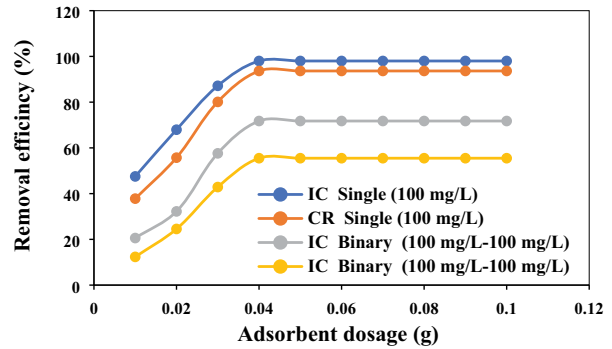


Fig. S2. Effect of adsorbent dosage of LDH on the removal efficiency of Zn<sub>2</sub>Al-LDH for IC and CR in single and binary systems.

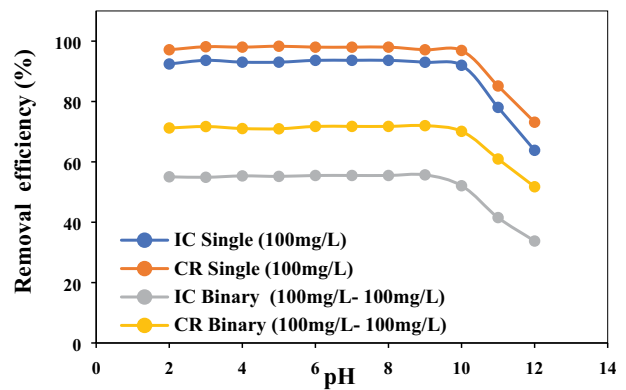


Fig. S3. Effect of initial pH on the removal efficiency of Zn<sub>2</sub>Al-LDH for IC and CR in single and binary systems.

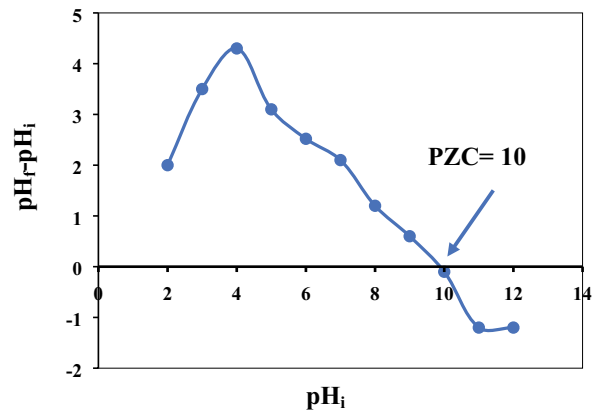


Fig. S4. Point of zero charge p<sub>H<sub>i</sub></sub>(<sub>pzc</sub>) of Zn<sub>2</sub>Al-LDH material.